



Full Text View

[Volume 32, Issue 9 \(September 2002\)](#)
Journal of Physical Oceanography

 Article: pp. 2492–2508 | [Abstract](#) | [PDF \(3.01M\)](#)

A Climatological Interpretation of the Circulation in the Western South Pacific*

Tangdong Qu
International Pacific Research Center, SOEST, University of Hawaii at Manoa, Honolulu, Hawaii
Eric J. Lindstrom
Office of Earth Science, National Aeronautics and Space Administration, Washington, D.C

(Manuscript received June 20, 2001, in final form January 15, 2002)

DOI: 10.1175/1520-0485(2002)032<2492:ACIOTC>2.0.CO;2

ABSTRACT

Time-averaged circulation is examined using historical hydrographic data near the Australia and Papua New Guinea coast in the Pacific. By averaging the data along isopycnal surfaces in a $0.5^\circ \times 0.5^\circ$ grid, the authors are able to show many detailed phenomena associated with the narrow western boundary currents, including the vertical structure of the bifurcation latitude of the South Equatorial Current (SEC) and the connection between the Solomon and Coral Seas. The bifurcation latitude of the SEC is found to move southward from about 15°S near the surface to south of 22°S in the intermediate layers. The origin of the Great Barrier Reef Undercurrent (GBRUC) is identified to be at about 22°S . Farther to the north, the GBRUC intensifies underlying the surface East Australian Current, and merges with the North Queensland Current (NQC) at about 15°S . The NQC turns eastward to flow along the Papua New Guinea coast and feeds into the New Guinea Coastal Undercurrent (NGCUC) through the Louisiade Archipelago. Further analysis shows that there is a strong water property connection between the Coral and Solomon Seas, confirming the earlier speculation on the water mass origins of the NGCUC.

1. Introduction

Hypotheses to account for Pacific decadal variability involve changes in the shallow, meridional circulation cells that allow exchange of waters between

Table of Contents:

- [Introduction](#)
- [Data and methods of analysis](#)
- [Vertically integrated](#)
- [Vertical structure of](#)
- [Bifurcation of the SEC](#)
- [Connection between the](#)
- [General characteristics](#)
- [Summary](#)
- [REFERENCES](#)
- [APPENDIX](#)
- [FIGURES](#)

Options:

- [Create Reference](#)
- [Email this Article](#)
- [Add to MyArchive](#)
- [Search AMS Glossary](#)

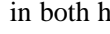
Search CrossRef for:


- [Articles Citing This Article](#)

Search Google Scholar for:


- [Tangdong Qu](#)
- [Eric J. Lindstrom](#)

the main oceanic gyres, namely the subtropical cells (STCs: [McCreary and Lu 1994](#)). In a zonal average, these cells consist of subduction in the subtropical gyres, equatorward flow at the thermocline and upper-intermediate levels, equatorial upwelling, and surface return flow back to the subtropics. Much of the subsurface, equatorward flow is presumed to occur in the low-latitude western boundary currents (LLWBCs: [Fine et al. 1994](#); [Lu and McCreary 1995](#)), while evidence also exists to suggest a possible pathway in the interior ocean ([Johnson and McPhaden 1999](#)). Variations in the strength or water mass properties of these subsurface, equatorward flow will, in due course, first influence the structures of the equatorial thermocline and cold tongue, and thereby feedback to affect the atmospheric circulation. Such slowly evolving STC variability, together with rapid atmospheric links between the Tropics and subtropics, have been hypothesized to be important in determining Pacific decadal climate variability ([Gu and Philander 1997](#); [Kleeman et al. 1999](#)).

The strength of the equatorward-flowing LLWBCs depends critically on the latitudes where the North and South Equatorial Currents (NEC and SEC) bifurcate at the western boundary. The precise location of these bifurcation latitudes determines the amount of subtropical water imported to the Tropics via the LLWBCs. According to Sverdrup theory, the bifurcation of the NEC and SEC should occur at the zero zonally integrated wind stress curl line situated at about 15° latitude in both hemispheres ([Fig. 1](#) ). This simple steady-state, depth-averaged theory, however, is not sufficient to describe the actual flow field, which is highly variable both in time and space. In the Northern Hemisphere, the NEC bifurcation occurs at a mean latitude of about 13°N near the surface ([Toole et al. 1990](#)), but it reaches as far north as 20°N in the intermediate layers ([Qu et al. 1998, 1999](#)). As a consequence, a subsurface countercurrent, namely the Luzon Undercurrent (LUC: [Qu et al. 1997](#)), is observed to flow southward underlying the Kuroshio, by which a significant amount of the North Pacific Intermediate Water is advected toward the equator along the east coast of Luzon ([Talley 1993](#); [Bingham and Lukas 1994](#); [Qu et al. 1999](#)). The appearance of the LUC has been linked with the basin-scale circulation of the North Pacific subtropical gyre that contracts poleward with depth ([Reid and Arthur 1975](#); [Qu 2001](#)).

Compared with its Northern Hemisphere counterpart, the depth distribution of the SEC bifurcation is less understood. Based on a set of hydrographic sections adjacent to the Great Barrier Reef at 18°S, [Church and Boland \(1983\)](#) found that the southward-flowing East Australian Current (EAC) begins at lower latitude at the surface than at the deeper levels and that the Great Barrier Reef Undercurrent (GBRUC) is a permanent feature at depths of 300–900 m. Later observations (e.g., [Church 1987](#); [Andrews and Clegg 1989](#)) and modeling studies (e.g., [de Szoeke 1987](#)) indicated that the bifurcation of the SEC occurs at a mean latitude of 18°–20°S, and this confirmed the earlier estimates given by [Wyrki \(1962\)](#) and [Scully-Power \(1973\)](#). Although the large-scale circulation of the western South Pacific has been broadly described in the previous studies using various synoptic observations (see a review by [Church and Craig 1998](#)), the detailed structure of the SEC bifurcation is unclear at this stage, and this situation seems to be complicated by the presence of New Caledonia, Vanuatu, and many other shallow topography features in the region ([Fig. 2](#) ; [Webb 2000](#)).

Near the equator, the vertical sections of currents along 133.5° and 137°E presented by [Masuzawa \(1968\)](#) illustrated the existence of the shallow eastward and southeastward Northwest Monsoon Current, overlying the strong northwestward flow of what we now know to be the New Guinea Coastal Undercurrent (NGCUC). Later observations ([Lindstrom et al. 1987](#); [Tsuchiya et al. 1989](#); [Murray et al. 1995](#)) suggested that the NGCUC is the primary source for the Equatorial Undercurrent and the NGCUC in turn must originate from the south, via the Solomon and Coral Seas. [Lindstrom et al. \(1987\)](#) speculated that there is a quasi-continuous coastal current that flows from about 20°S northward along the coast of Australia, clockwise through the Gulf of New Guinea, and northward into the Solomon Sea near the Louisiades. While evidence does exist for this speculation (e.g., [Church 1987](#); [Tsuchiya et al. 1989](#); [Lindstrom et al. 1990](#); [Cresswell 2000](#)), the connection between the NGCUC and the GBRUC has never been carefully examined due to sporadic sampling of this current system.

Dynamic heights calculated from the *World Ocean Atlas 1998* (WOA98, available online at www.nodc.noaa.gov/OC5/indprod.html) by assuming a 1200-db reference level clearly demonstrate the poleward shift of the SEC with increasing depth ([Fig. 3](#) ) , as shown in [Reid's \(1986, 1997\)](#) absolute flow fields. Near the sea surface, the SEC is dominated by a broad northwestward flow that crosses the equator over much of the Pacific basin. Below the sea surface, the SEC becomes west–east oriented and is found farther poleward, extending to about 25°S at depth 300 m and 30°S at 800 m. As already noted by many earlier studies (e.g., [Qu et al. 1999](#)), this climatological dataset is problematic near the western boundary and thus fails to resolve the narrow western boundary currents adequately, as a result of smoothing over more than 700 km.

This study seeks to provide a time-average, three-dimensional picture of the circulation in the western South Pacific. We utilize all historical hydrographic data and carry out an analysis of the SEC, GBRUC, and NGCUC in a physically consistent way. Our special attention will be paid to the depth distribution of the SEC bifurcation latitude and the connection between the Solomon and Coral Seas through the narrow western boundary currents. The results of this analysis are presented in the following sections. In [section 2](#), we describe the data and methods of analysis. In [section 3](#), we show vertically integrated circulation. In [section 4](#) we provide a three-dimensional picture of the circulation and in [section 5](#) examine the depth dependence of the SEC bifurcation. The connection between the Coral Sea and Solomon Sea is illustrated in [section 6](#), and the large-scale characteristics of water masses are described in [section 7](#). Results are summarized in [section 8](#), and an error analysis is made in the [appendix](#).

2. Data and methods of analysis

For this study CTD and bottle profiles at observed levels recorded on the CD-ROMs of World Ocean Database 1998 (NOAA 1998) from the region 40°S–0°, 140°E–180° are used. Taking advantage of the previous analyses (Levitus 1982, 1994), those profiles (3455) that failed to pass the monthly, seasonal, and annual standard deviation checks are excluded from the start. Then, we select the data by the removal of profiles (26 541) shallower than 100 m, profiles (631) with obviously erroneous records (e.g., temperature higher than 10°C below 800 m, salinity greater than 34.7 psu between 800 and 1200 m, or oxygen concentration larger than 8 ml l⁻¹ below 100 m), and profiles with only a few measurements in the shallow (<100 m) and deep (>500 m) layers but without any measurements in between. After all these procedures of quality control, the final dataset used for this study consists of 18 706 profiles of temperature/salinity and 14 897 profiles of oxygen (Fig. 4 ●). The data coverage is generally good. In comparison with its Northern Hemisphere counterpart, the upper ocean is better sampled near the coast of Australia than near the coast of Philippines (Qu et al. 1999), despite the lack of Southern Hemisphere data as a whole. The spatial distribution of the data for each season is much the same (not shown); no obvious bias in density of sampling is apparent toward any season of the year.

Water properties at observed levels are first interpolated onto a set of density surfaces with a 0.02 kg m⁻³ vertical resolution using cubic spline, and then averaged in a 0.5° × 0.5° grid, regardless of the data and time of observation. The number of samples is usually more than five at each grid cell and can be as many as several tens, even several hundreds, near the coast of Australia. For the region where data coverage is relatively sparse, we smooth the property fields by choosing a horizontal radius big enough to include at least five observations at high latitudes (10°–40°S) and 20 observations in the tropical region to reduce the dynamic height noise amplified by the smallness of Coriolis parameter. The concept of averaging on isopycnal surfaces breaks down at the sea surface due to the outcropping of shallower isopycnals. As has been done previously (Gouriou and Toole 1993; Qu et al. 1999), the average properties between the mean mixed layer depth (defined as the first depth at which the potential density is 0.1 kg m⁻³ greater than the surface value) and the first isopycnal surface present on all profiles are obtained by linear interpolation.

Standard deviations of properties are also estimated during averaging (see the appendix for details) and used to edit the mean fields. If an interpolated property deviates from the grid mean by a value three times larger than the standard deviation, it is excluded, and the mean and standard deviation are recalculated. The averaged properties are finally smoothed using a Gaussian filter with *e*-folding scales of about 100 km, and interpolated back to a 10-db uniform pressure series in the upper 1200 m.

The mean temperature and salinity are then converted to dynamic height on pressure surfaces and/or acceleration potential on isopycnal surfaces, from which geostrophic flow is derived. While deeper observations are available at some locations and times, the number of samples decreases rather rapidly with depth. To optimize uniformity of the database, we select the reference level at 1200 db or at the bottom of the ocean where water depth is shallower. Given that the present study is restricted to the circulation and water mass distribution in the upper 1000 m alone, this selection of reference level is reasonable.

3. Vertically integrated circulation

Depth-integrated dynamic height, defined as

$$P = \frac{1}{g} \int_{1000\text{db}}^0 D dz,$$

provides an overview of the vertically integrated circulation in the upper ocean (Fig. 5 ●), where *D* represents dynamic height at depth *z* relative to 1200 db and *g* is the acceleration due to gravity. In the region between 10° and 20°S, the vertically integrated circulation is dominated by a westward flow associated with the SEC, forming the boundary between the tropical and subtropical gyres. This westward flow splits as it encounters the western boundary into the northward-flowing North Queensland Current (NQC) and the southward-flowing EAC. The NQC is continuous to the north as a swift and narrow western boundary current, supplying waters of subtropical origin into the NGCUC. Most of the EAC leaves the Australian coast and flows into the deep ocean at 30°–35°S, in reasonable agreement with earlier observations (Godfrey et al. 1980), while the rest continues to the south reaching as far as the east coast of Tasmania (beyond the region of studied here: Ridgway and Godfrey 1994). Some of the eastward flow returns to the north and forms a tight recirculation gyre, and some continues to flow eastward, forming the southern boundary of the subtropical gyre.

Also evident in Fig. 5 ● is a tongue of low dynamic height (<750 m²) extending westward from the dateline along 10°–12°S, indicative of a narrow eastward flow associated with the South Equatorial Countercurrent (SECC: Reid 1959, 1965; Tsuchiya 1968) on its northern side. This eastward flow appears to start near the Solomon Islands and is connected with the

SEC by several small-scale recirculations. In the latitude band where the Solomon Islands stretch, roughly between 5° and 10°S, the SEC is blocked and it makes southward deflections east of these islands, where part of it appears to turn eastward and feed into the SECC.

The bifurcation of the SEC, defined as where the meridional transport within a 2° longitude band from the continental slope is zero, occurs at 17.8°S. If surface Ekman transport is considered, it moves slightly northward to 17.7°S. These values are in reasonable agreement with earlier observations (Scully-Power 1973; Church 1987) but almost 3° farther southward than that predicted by Sverdrup theory (Fig. 1). Given the presence of New Caledonia, Vanuatu, Queensland Plateau, and many other small islands and reefs in the region (Fig. 2), this discrepancy might be interpreted in part as a result of blocking by shallow topography (Webb 2000). Here, however, we emphasize also the importance of the Indonesian Throughflow (ITF) in determining the bifurcation latitude of the SEC. Godfrey (1989) argued that the ITF is a component of the circulation around Australia–Papua New Guinea, considered as an island isolated by the deep passages through the Indonesian archipelago, and because of this circulation the transport of the EAC must be altered. Indeed, a net northward transport of 14 Sv ($\text{Sv} \equiv 10^6 \text{ m}^3 \text{ s}^{-1}$) has been observed across the South Pacific at 28°S (Godfrey and Golding 1981). A part of this northward transport may occur at the western boundary, reducing the transport of the EAC, augmenting the region of equator-flowing NQC/NGCUC, and pushing the SEC bifurcation latitude farther southward, with the rest occurring in the interior ocean (de Szoeke 1987). In our dynamic topography field (Fig. 5), the discrepancy between the observed SEC bifurcation latitude and the zero zonally integrated wind stress curl line suggests a northward transport of about 2 Sv within a 2° longitude band from the continental slope. This value might be underestimated as a result of smoothing in preparing this dataset.

4. Vertical structure of the circulation

a. Horizontal maps

Time-averaged dynamic height (relative to 1200 db) and its derived geostrophic flow (Fig. 6) are presented to show the vertical structure of the circulation in the western South Pacific. At the sea surface, the signature of westward flow is almost unrecognizable, except near the northern boundary of the region where the northern branch of the SEC spans from the equator to about 8°S (Kessler and Taft 1987). Over a large part of the region south of 20°S, the surface current seems to be dominated by a weak eastward flow (discussed in section 4b). Near the western boundary, the EAC flows southward at speeds of order 20 cm s^{-1} , supplying waters into the eastward flow of the interior ocean. The accumulation of the southwestward-flowing Ekman current (not shown) against the coast appears to act as a primary water source for the NQC and EAC in the surface layer. In response to the seasonally reversing monsoon, the surface New Guinea Coastal Current (NGCC) is rather weak, and as a result, much of the NQC appears to proceed eastward into the SECC.

The SEC becomes better defined at 100 m. In the open ocean, a narrowly confined westward flow associated with the SEC exists between 12° and 17°S, and the eastward flow shown at the sea surface between 20° and 35°S is somewhat weaker and retreats farther south. Along the western boundary, the SEC bifurcates at about 15°S (discussed in section 5). Most of its northern branch (i.e., the NQC) appears to turn northwestward around the Louisiade archipelago (discussed in section 6) and enter the equatorial ocean as part of the NGCUC through the Vitiaz Strait; no eastward turning of the NQC is apparent at this depth.

The SECC is observed as a narrow eastward flow between 8° and 11°S with a maximum speed of the order 10 cm s^{-1} within 200 m of the sea surface. Two pathways are identified to contribute to the SECC. One is the southward deflection of the SEC in the latitudes between 5° and 10°S. As it has been indicated in the depth-integrated dynamic height field (Fig. 5), part of the SEC at this latitude band turns into the eastward-flowing SECC through several small-scale recirculations before reaching the Solomon Islands. Another contribution to the SECC is from the eastward turning of the NQC. Near the sea surface, the NGCC reverses its direction twice a year in response to the monsoonal wind (Lindstrom et al. 1987), and on the annual average, only a small part of it passes through the Vitiaz Strait into the equatorial ocean, with the rest turning eastward to feed the SECC.

The SEC is fully developed at depths around 300 m, leading to an enhanced NGCUC with its maximum speed exceeding 20 cm s^{-1} . South of 10°S the SEC becomes much stronger and extends to about 20°S; north of it the SEC is seen only in a narrow latitude band near 5°S and the SECC has disappeared at this depth. Near the western boundary, we also see a major change to the EAC, which starts to appear somewhat farther south and is much weaker compared with the case discussed for the shallower waters.

The SEC continues to move southward at increasing depths (500–1000 m), reaching as far south as 30°S at 1000 m. North of 15°S, there is no westward flow below 500 m, and a weak eastward flow starts to appear around 800 m, extending from the Solomon Sea into the central Pacific. The presence of this weak eastward flow might be related to the narrowing of the Vitiaz Strait at deeper levels. Careful examination of bottom topography indicates that the maximum depth of the Vitiaz strait is about 1000 m, so significant blocking by shallower topography is expected around that depth. In

response, a large part of the NQC turns eastward after passing through the Louisiade archipelago, and eventually forms the unnamed eastward-flowing current as shown in [Fig. 6](#).

An important aspect of the velocity field ([Fig. 6](#)) is that the SEC does not appear to be simply a broad, one-cell westward flow as was traditionally considered. This large-scale westward flow is actually blocked by a number of islands and other topography features. Extensive blocking effect of shallow topography has been reported in recent model simulations. Among others, [Webb \(2000\)](#) shows that the SEC is broken up into a series of westward flow cells as it enters the Coral Sea. The present results lend additional support for those suggested by Webb, though such a blocking effect is much reduced here as a result of smoothing. The presence of New Caledonia and several small reefs to the west, for example, blocks the westward extension of the SEC at latitudes between 20° and 25°S, and as a result, two cells of the zonal flow are formed extending westward from the northern and southern extremities. This blocking naturally induces a bifurcation of the SEC, with the northern cell flowing northwestward to feed the GBRUC and the southern cell flowing southwestward to feed the EAC.

b. Vertical sections

Velocity sections are presented to show the structure of zonal flow along 160°E and 170°E ([Fig. 7](#)). Near the sea surface, geostrophic flow is generally weak, and this seems to agree with the early work of [Wyrski \(1975\)](#), [Tsuchiya \(1982\)](#), [Andrews and Clegg \(1989\)](#), and [Reid \(1997\)](#). At 170°E, westward flow associated with the SEC occurs only in a narrow band from 12° to 17°S; farther southward, there exists a broad eastward flow extending from about 17°S to the southern end of the section at 35°S, as already indicated in [Fig. 6](#). This eastward flow corresponds to the “South Tropical Countercurrent” first referred to by [Merle et al. \(1969\)](#); but later studies suggest that it represents only the northern edge of the eastward flow in the poleward side of the subtropical gyre and not a countercurrent (e.g., [Wyrski 1975](#); [Tsuchiya 1982](#)). At 160°E, similar structure is found, except that the surface eastward flow appears to be somewhat farther southward. Several small-scale phenomena are also seen reflecting the blocking effect of shallow topography around 9° and 25°S.

The two branches of the SEC are clearly indicated in the sections of zonal velocity. In the south, the core of the SEC is observed near 13°S, exceeding 6 cm s^{-1} at depths of 100–200 m. The velocity core deepens to the south, falling below 600 m at latitudes around 25°S, where its magnitude drops to near 1 cm s^{-1} . Two narrow westward jets are identified as local velocity cores: one lies at about 600 m near 25°S, and the other lies at about 300 m near 19°S, reflecting the effect of shallow topography associated with New Caledonia and several small islands and reefs to the west. The northern branch of the SEC is shallower and its maximum velocity exceeds 10 cm s^{-1} around 5°S.


As already shown in [Fig. 6](#), the SECC flows eastward as a single connected flow confined above 200 m, and is underlain by weak westward flow connecting the two branches of the SEC at about 200–400 m ([Fig. 7](#)). The meridional extent of the SECC is limited within about 4° of latitude. Deeper in the water column (below 400 m), the flow turns eastward again. To the best of our knowledge, this deep eastward flow has not been previously reported. [Reid's \(1997\)](#) dynamic height maps (his Fig. 5) have indeed shown an eastward flow below 500 m, but its location is somewhat farther north (2°–6°S).


5. Bifurcation of the SEC


The dynamic height and geostrophic flow fields have shown the large-scale behavior of the SEC in the western South Pacific, with its axis moving southward at increasing depth. An important result related to this southward shift of the SEC is its depth dependence of bifurcation latitude along the western boundary. To further illustrate the vertical structure of the bifurcation and its correspondence with the LLWBCs, we show six velocity sections at every 2° of latitude from 23° to 13° S along the continental slope east of Australia ([Fig. 8](#)). At 23°S, the EAC stands out as a southward flow at all depths in the upper 1000 m. The GBRUC originates between 23° and 21°S, about 4° farther southward than previously observed (e.g., [Church and Boland 1983](#)). It is first detectable at 21°S, with a maximum speed exceeding 0.5 cm s^{-1} at about 600–700 m. At 19°S, the GBRUC continues to exist, but extends slightly deeper than that shown at 21°S presumably due to the presence of the Queensland Plateau. Further to the north, the GBRUC intensifies and eventually merges with the NQC at about 13°S.

The bifurcation latitude of the SEC, by definition, is the place where the western boundary currents reverse. The meridional shift of the bifurcation latitude is pronounced ([Fig. 9](#)), moving from about 15°S near the surface to about 22° S at depths around 800 m. Within the latitude band where the bifurcation of the SEC occurs, namely between about 15° and 22°S, the GBRUC flows northward underneath the southward-flowing EAC, until it merges with the NQC.

6. Connection between the Coral Sea and Solomon Sea



The discovery of the NGCUC confirms [Tsuchiya's \(1968\)](#) hypothesis on the water mass origins of the Equatorial Undercurrent in the western Pacific. The water in the NGCUC in turn must come from the south via the Solomon and Coral Seas ([Lindstrom et al. 1987](#)). Indeed, we see that there is a flow connecting the Coral Sea and Solomon Sea around the Lousiade archipelago ([Fig. 10](#) ). This flow starts in the vicinity of the GBRUC in the western Coral Sea, turns eastward along the south coast of Papua New Guinea, and enters the Solomon Sea through the Lousiade archipelago to feed the NGCUC. The maximum speed of the flow ($>8 \text{ cm s}^{-1}$) lies at 200–300 m, and this, to a certain extent, is consistent with the idea that the Coral Sea and Solomon Sea are connected by undercurrents ([Lindstrom et al. 1987](#)).

Water mass properties in the upper 1000 m are continuous along the south coast of Papua New Guinea and the western boundary of the Solomon Sea. On density surfaces around $\sigma_\theta = 25.0$, we see a core of high salinity ($>35.65 \text{ psu}$) and low oxygen concentration extending toward the coast, indicative of the influence of the South Pacific Tropical Water (SPTW) in the ocean interior ([Fig. 11](#) ). Water near the continental slope has relatively lower salinity and higher oxygen concentration, consonant with its supply from the subtropical gyre. In the intermediate layers, low salinity ($<34.5 \text{ psu}$) water characteristic of the Antarctic Intermediate Water (AAIW) also enters the Solomon Sea following the NQC/NGCUC.


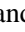
The water property connection between the Coral Sea and Solomon Sea is also evident in the relations of temperature versus salinity, temperature versus oxygen concentration, and salinity versus oxygen concentration of water masses. Here, 313 profiles at observed levels in a box selected south of New Guinea between 9° and 14°S , 146° and 151°E are used for the Coral Sea, and 169 profiles are used for the Solomon Sea. Except for a shallow surface layer where $T > 25^\circ\text{C}$ and $\text{O}_2 > 4 \text{ ml l}^{-1}$, the characteristics of water masses in these two areas are quite similar ([Fig. 12](#) ). The SPTW is seen as a salinity maximum ($>35.5 \text{ psu}$) at $20^\circ < T < 25^\circ\text{C}$ and $\text{O}_2 \sim 3.5 \text{ ml l}^{-1}$ around $24.5 \sigma_\theta$. Below that depth, temperature and salinity decrease with depth, but oxygen concentration remains much the same until reaching the AAIW at about $\sigma_\theta = 27.2$ that marks the bottom of ventilated thermocline water.

7. General characteristics of water masses


a. Sectional distributions


Maps of potential temperature, salinity, potential vorticity, and oxygen concentration are shown against density along 160°E and 170°E ([Figs. 13](#)  and [14](#) ). On both sections, the high salinity ($20^\circ\text{C} < T < 25^\circ\text{C}$, $S > 35.65 \text{ psu}$) SPTW is seen lying around $24.5 \sigma_\theta$ surface (between 100 and 200 m in depth) in the north and connected to the surface layer in the south. The northern component of the SPTW (say, north of 15°S) comes as part of the SEC from the high salinity surface region centered at about 120°W , while the southern component with high oxygen values ($>4.8 \text{ ml l}^{-1}$) is associated with the high salinity surface outcrop region near 30°S , 180° (e.g., [Wyrki 1962](#); [Tsuchiya 1982](#); [Reid 1997](#)).


The distribution of potential vorticity reveals the existence of the South Pacific Subtropical Mode Water (STMW) on density surfaces between 25.8 and $26.2 \sigma_\theta$. The formation of the STMW is associated with large surface buoyancy loss caused by intense surface cooling in winter north of New Zealand ([Roemmich and Cornuelle 1992](#); [Hanawa and Talley 2001](#)). As a result of its convective origin, in the density range of STMW there is a thick layer of low potential vorticity ($< 2.5 \times 10^{-10} \text{ m}^{-1} \text{ s}^{-1}$ in magnitude), corresponding with relatively homogenous oxygen distribution ($4.2 < \text{O}_2 < 4.4 \text{ ml l}^{-1}$).

Deeper in the water column, the AAIW stands out as a salinity minimum ($<34.5 \text{ psu}$) emanating from the south along density surface centered at $27.2 \sigma_\theta$, and resides on a strong vertical gradient of oxygen concentration ([Figs. 13](#)  and [14](#) ). This low salinity ($<34.5 \text{ psu}$), high oxygen ($>4.0 \text{ ml l}^{-1}$) water is formed in the southeast Pacific and is carried into the west ocean by the deep extension of the SEC ([Reid 1965](#); [Talley 1999](#)).

b. Horizontal distributions

Maps of temperature, salinity, isopycnal surface, oxygen concentration, potential vorticity, and acceleration potential are presented to provide direct pathways of the SPTW, STMW, and AAIW on 24.5 , 26.0 , and $27.2 \sigma_\theta$ surfaces, respectively ([Fig. 15](#) ). The $24.5 \sigma_\theta$ surface passes through the upper thermocline at depths 100–180 m in the Tropics (5° – 20°S) and outcrops the sea surface in the subtropics around 30°S . Property distribution on this isopycnal surface is dominated by the spreading of the SPTW. This high temperature ($>23^\circ\text{C}$), high salinity ($>35.7 \text{ psu}$), low oxygen concentration ($<3.5 \text{ ml l}^{-1}$), and low potential vorticity ($< 5 \times 10^{-10} \text{ m}^{-1} \text{ s}^{-1}$) water is advected westward via the SEC and exerts strong influence on the water masses in the Coral Sea and Solomon Sea as shown in [section 6](#).

The $26.0 \sigma_\theta$ surface bowls down below 300 m over a large part of the subtropical gyre, ridges up to about 200 m near the equator, and outcrops the sea surface at 40° – 45° S (WOA98). The STMW characterized by high temperature ($>16.5^\circ\text{C}$), high salinity (>35.48 psu), high oxygen concentration ($>4.5 \text{ ml l}^{-1}$), and low potential vorticity ($<2.25 \times 10^{-10} \text{ m}^{-1} \text{ s}^{-1}$ in magnitude) enters the west ocean at latitudes roughly between 23° and 28° S, associated with the EAC extension recirculation gyre (Fig. 15 ). Much of the STMW is advected eastward via the eastward extension of the EAC and flows into the subtropical gyre in the central Pacific (outside the region plotted here).

Property distribution on the $27.2 \sigma_\theta$ surface is dominated by the northwestward spreading of the AAIW from its formation region in the southeast Pacific (Reid 1965, 1986, 1997). Compared with the case discussed for the STMW, the AAIW with typical values of $T < 5.2^\circ\text{C}$, $S < 34.45$ psu, $\text{O}_2 > 4.2 \text{ ml l}^{-1}$, and $\text{PV} \sim -0.6 \times 10^{-10} \text{ m}^{-1} \text{ s}^{-1}$ extends farther northward (Fig. 15 ). At the western boundary, some of this water is advected into the Solomon Sea following a pathway of GBRUC, NQC, and NGCUC.

8. Summary

This study provides a time-averaged, three-dimensional picture of the circulation in the western South Pacific. Unlike most previous climatological analyses (e.g., Levitus 1982, 1994), we average the data along isopycnal instead of pressure surfaces and use smaller smoothing scales. This approach reveals a more detailed phenomenology associated with the narrow western boundary currents. Although some of the phenomena are already known from sporadic observations, they have not been represented heretofore in a physically consistent way.

The vertically integrated circulation shows a bifurcation latitude of the SEC around 18° S, about 3° south of that required by Sverdrup constraint. This result differs from its counterpart in the Northern Hemisphere, where the observed and predicted vertically integrated bifurcation latitude of the NEC are in reasonable agreement. In addition to the blocking effect of bottom topography, this result reflects the importance of the ITF in determining the bifurcation latitude of the SEC at its western terminal.

We do not interpret the SEC as simply a broad, one-cell westward flow. Rather, at the surface, it is generally weak and narrow, and the total surface flow is actually dominated by the Ekman current. Below the surface, it contains multiple cores of velocity ranging in depth from 100–200 m near 13° S to 600–700 m near 22° S.

The bifurcation latitude of the SEC is found to move southward from about 15° S near the surface to about 22° S in the upper intermediate layers. As a result, the GBRUC starts to appear as a subsurface countercurrent around 22° S. This subsurface countercurrent shoals with its core from 600 to 800 m at its origin to 300–400 m at 15° S before it merges into the NQC and eventually into the NGCUC. The connection between the GBRUC and NQC/NGCUC is quite similar to that between the LUC and MC in the Northern Hemisphere.

The focus of the present study is on the time-averaged structure of the circulation near the Australia and Papua New Guinea coast in the Pacific. We must recognize that specific cruise data indicate currents with significant time variability. This variability, however, is not yet resolvable with the accumulated data.

The results of this analysis suggest that there is a strong water property connection between the Coral Sea and Solomon Sea. Both SPTW and AAIW can be traced continuously in the flow path of GBRUC, NQC, and NGCUC, giving positive evidence for the hypothesis that the NGCUC originates from the south via the Coral and Solomon Seas.

Acknowledgments

This research was supported by Frontier Research System for Global Change through its sponsorship of the International Pacific Research Center and by the National Science Foundation through Grant OCE00-95906. TQ is grateful to J. P. McCreary, H. Mitsudera, T. Jensen, and T. Miyama for many valuable discussions. Thanks are also extended to G. Meyers, T. Yamagata, and J. Church for useful communication on the present topic, and to L. Talley and two anonymous reviewers from useful comments on the earlier manuscript.

REFERENCES

Andrews J. C., and S. Clegg, 1989: Coral Sea circulation and transport deduced from modal information models. *Deep-Sea Res.*, **36**, 957–974. [Find this article online](#)

Bingham F. M., and R. Lukas, 1994: The southward intrusion of North Pacific Intermediate Water along the Mindanao coast. *J. Phys.*

Church J. A., 1987: The East Australian Current adjacent to the Great Barrier Reef. *Aust. J. Mar. Freshwater Res.*, **38**, 671–683. [Find this article online](#)

Church J. A., and F. M. Boland, 1983: A permanent undercurrent adjacent to the Great Barrier Reef. *J. Phys. Oceanogr.*, **13**, 1747–1749. [Find this article online](#)

Church J. A., and P. D. Craig, 1998: Australia's shelf seas: Diversity and complexity. *The Sea*, Vol. 11, *The Global Coastal Ocean: Regional Studies and Syntheses*, A. R. Robinson and K. H. Brink, Eds., Wiley and Sons, 933–964.

Cresswell G. R., 2000: Coastal currents of northern Papua New Guinea, and the Sepil River outflow. *Mar. Freshwater Res.*, **51**, 553–564. [Find this article online](#)

De Szoek R. A., 1987: On the wind-driven circulation of the south Pacific Ocean. *J. Phys. Oceanogr.*, **17**, 613–630. [Find this article online](#)

Fine R., R. Lukas, F. M. Bingham, M. J. Warner, and R. H. Gammon, 1994: The western equatorial Pacific is a water mass crossroads. *J. Geophys. Res.*, **99**, 25063–25080. [Find this article online](#)

Godfrey S. J., 1989: A Sverdrup model of the depth-integrated flow for the world ocean allowing for island circulations. *Geophys. Astrophys. Fluid Dyn.*, **45**, 89–112. [Find this article online](#)

Godfrey S. J., and T. J. Golding, 1981: The Sverdrup relation in the Indian Ocean, and the effect of Pacific–Indian Ocean throughflow on Indian Ocean circulation and on the East Australia Current. *J. Phys. Oceanogr.*, **11**, 771–779. [Find this article online](#)

Godfrey S. J., G. R. Cresswell, T. J. Golding, A. F. Pearce, and R. Royd, 1980: The separation of the East Australian Current. *J. Phys. Oceanogr.*, **10**, 430–440. [Find this article online](#)

Gouriou Y., and J. Toole, 1993: Mean circulation of the upper layers of the western equatorial Pacific Ocean. *J. Geophys. Res.*, **98**, 22495–22520. [Find this article online](#)

Gu D., and S. G. H. Philander, 1997: Interdecadal climate fluctuations that depend on exchange between the tropics and extratropics. *Science*, **275**, 805–807. [Find this article online](#)

Hanawa K., and L. D. Talley, 2001: Mode waters. *Ocean Circulation and Climate*, G. Siedler, J. Church, and J. Gould, Eds., Academic Press, 373–386.

Hellerman S., and M. Rosenstein, 1983: Normal monthly wind stress over the world ocean with error estimates. *J. Phys. Oceanogr.*, **13**, 1093–1104. [Find this article online](#)

Johnson G. C., and M. J. McPhaden, 1999: Interior pycnocline from the subtropical to the equatorial Pacific Ocean. *J. Phys. Oceanogr.*, **29**, 3073–3089. [Find this article online](#)

Kessler W. S., and B. A. Taft, 1987: Dynamic heights and zonal geostrophic transports in the central tropical Pacific during 1979–1984. *J. Phys. Oceanogr.*, **17**, 97–122. [Find this article online](#)

Kleeman R., J. P. McCreary, and B. A. Klinger, 1999: A mechanism for generating ENSO decadal variability. *Geophys. Res. Lett.*, **26**, 1743–1746. [Find this article online](#)

Levitus S., 1982: *Climatological Atlas of the World Oceans*. NOAA Prof. Paper 13, 173 pp. and 17 microfiche.

Levitus S., 1994: *World Ocean Atlas 1994*. Vol. 13, National Oceanographic Data Center, CD-Rom.

Lindstrom E., R. Lukas, R. Fine, E. Firing, S. J. Godfrey, G. Meyers, and M. Tsuchiya, 1987: The western equatorial Pacific Ocean circulation study. *Nature*, **330**, 533–537. [Find this article online](#)

Lindstrom E., J. Butt, R. Lukas, and S. Godfrey, 1990: The flow through Vitiaz Strait and St. George's Channel, Papua New Guinea. *The Physical Oceanography of Sea Straits*, L. Pratt, Ed., Kluwer Academic, 171–189.

Lu P., and J. P. McCreary, 1995: Influence of the ITCZ on the flow of thermocline water from the subtropical to equatorial Pacific Ocean. *J. Phys. Oceanogr.*, **25**, 292–309. [Find this article online](#)

Masuzawa J., 1968: Second cruise for CSK, Ryofu Maru, January to March 1968. *Oceanogr. Mag.*, **20**, 173–185.

McCreary J. P., and P. Lu, 1994: On the interaction between the subtropical and the equatorial oceans: The subtropical cell. *J. Phys. Oceanogr.*, **24**, 466–497. [Find this article online](#)

Merle J., H. Rotschi, and B. Voituriez, 1969: Zonal circulation in the tropical western South Pacific at 170°E. *Bull. Japan Soc. Fish. Oceanogr.*, Special Issue (Prof. Uda's Commemorative Papers), 91–98.

Murray S., E. Lindstrom, J. Kindle, and E. Weeks, 1995: Transport through the Vitiaz Strait. *WOCE Notes*, **7**, 21–23.

NOAA., 1998: *World Ocean Database 1998*. NOAA/NODC, 5 CD-ROM disks.

Qu T., 2001: Depth distribution of the subtropical gyre in the North Pacific. *J. Oceanogr.*, **58**, 525–529. [Find this article online](#)

Qu T., T. Kagimoto, and T. Yamagata, 1997: A subsurface countercurrent along the east coast of Luzon. *Deep-Sea Res. I*, **44**, 413–423. [Find this article online](#)

Qu T., H. Mitsudera, and T. Yamagata, 1998: On the western boundary current in the Philippines Sea. *J. Geophys. Res.*, **103**, 7537–7548. [Find this article online](#)

Qu T., 1999: A climatology of the circulation and water mass distribution near the Philippine coast. *J. Phys. Oceanogr.*, **29**, 1488–1505. [Find this article online](#)

Reid J. L., 1959: Evidence of a South Equatorial Countercurrent in the Pacific Ocean. *Nature*, **184**, 209–210. [Find this article online](#)

Reid J. L., 1965: Intermediate waters of the Pacific Ocean. *Johns Hopkins Oceanogr. Stud.*, No. 2, 85 pp.

Reid J. L., 1986: On the total geostrophic circulation of the South Pacific Ocean: Flow patterns, traces and transports. *Progress in Oceanography*, Vol. 16, Pergamon, 1–61.

Reid J. L., 1997: On the total geostrophic circulation of the Pacific Ocean: Flow patterns, traces and transports. *Progress in Oceanography*, Vol. 39, Pergamon, 263–325.

Reid J. L., and R. S. Arthur, 1975: Interpretation of maps of geopotential anomaly for the deep Pacific Ocean. *J. Mar. Res.*, **33**, 37–52, (Suppl.). [Find this article online](#)

Ridgway K. R., and J. S. Godfrey, 1994: Mass and heat budgets in the East Australian Current: A direct approach. *J. Geophys. Res.*, **99**, 3231–3248. [Find this article online](#)

Roemmich D., and B. Cornuelle, 1992: The subtropical mode waters of the South Pacific Ocean. *J. Phys. Oceanogr.*, **22**, 1178–1187. [Find this article online](#)

Scully-Power P. D., 1973: Coral Sea flow budgets in winter. *Aust. J. Mar. Freshwater Res.*, **24**, 203–215. [Find this article online](#)

Talley L. D., 1993: Distribution and formation of North Pacific Intermediate Water. *J. Phys. Oceanogr.*, **23**, 517–537. [Find this article online](#)

Talley L. D., 1999: Some aspects of ocean heat transport by the shallow, intermediate and deep overturning circulation. *Mechanisms of Global Climate Change at Millennial Time Scales*, *Geophys. Monogr.*, No. 112, Amer. Geophys. Union, 1–22.

Toole J., R. C. Millard, Z. Wang, and S. Pu, 1990: Observations of the Pacific North Equatorial Current bifurcation at the Philippine coast. *J. Phys. Oceanogr.*, **20**, 307–318. [Find this article online](#)

Tsuchiya M., 1968: Upper waters of the intertropical Pacific Ocean. *Johns Hopkins Oceanogr. Stud.*, No. 4, 50 pp.

Tsuchiya M., 1982: On the Pacific upper-water circulation. *J. Mar. Res.*, **40**, 777–799. [Find this article online](#)

Tsuchiya M., R. Lukas, R. A. Fine, E. Firing, and E. Lindstrom, 1989: Source waters of the Pacific equatorial undercurrent. *Progress in Oceanography*, Vol. 23, Pergamon, 101–147.

Webb D. J., 2000: Evidence for shallow zonal jets in the South Equatorial Current region of the southwest Pacific. *J. Phys. Oceanogr.*, **30**, 706–720. [Find this article online](#)

Wyrtki K., 1962: The subsurface water masses in the western South Pacific. *Aust. J. Mar. Freshwater Res.*, **13**, 18–47. [Find this article online](#)

Wyrtki K., 1975: Fluctuations of the dynamic topography of the Pacific Ocean. *J. Phys. Oceanogr.*, **5**, 450–459. [Find this article online](#)

9. Error Analysis

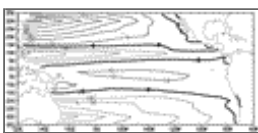
A measure of the uncertainty in the mean fields presented in this study is afforded by calculating standard deviations. At depths of the thermocline (say, on $\sigma_\theta = 25.0$), the standard deviations are large at the higher latitudes, namely south of 25°S , exceeding 0.3°C in temperature and 0.20 psu in salinity. These higher values of standard deviations clearly demonstrate the influence of the seasonal thermocline. Standard deviations drop dramatically to the north, and near the coast of Australia in particular they fall below 0.15°C and 0.05 psu in temperature and salinity in a broad latitude band of 25° – 5°S . The standard deviations close to the international date line are somewhat larger than those to the west due to sparse sampling of the ocean.

The spatial distribution of standard deviations is relatively uniform below the thermocline. On the $27.2 \sigma_\theta$ surface, for example, typical temperature and salinity standard deviations, defined as the spatial average over the domain, are 0.2°C and 0.03 psu. The standard deviations of oxygen concentration are also obtained, showing a pattern consistent with those of temperature and salinity. On the regional average, the standard deviations of oxygen concentration are of the order 0.25 ml l^{-1} at depths of the thermocline, and they decrease with depth, approaching about 0.15 ml l^{-1} at depths around $\sigma_\theta = 27.2$.

The estimates of standard deviations are based in most cases on ensembles of more than 10 samples collected in various seasons of different years. Part of the uncertainty in the mean fields is due to the time variations ranging from synoptic to decadal timescales. We note, however, this uncertainty could also be attributed to the bad quality of the data. For one reason, most of the observations used for this study were made at conventional standard depths, and as a result, the interpolation of properties onto isopycnal surfaces may be subject to uncertainty. For the second, sparse data coverage may enhance the uncertainty by using a larger radius of averaging in some parts of the region, and this seems to be the case around the international date line.

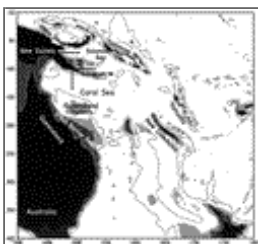
Although there is no easy way to definitely know how much of the uncertainty cited above is due to time variations and how much is due to the errors in the data, their effect on the mean fields are expected to be much reduced by the combined use of observations from different seasons of different years. So, we feel that most of the large-scale phenomena of the circulation described in this study are representative. They are unlikely to be modified in a qualitative sense, though quantitative changes are likely as more data become available.

Figures



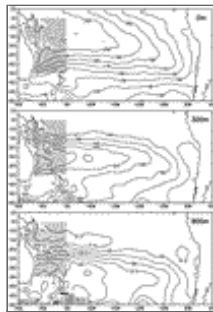
[Click on thumbnail for full-sized image.](#)

FIG. 1. Sverdrup transport (Sv) calculated from [Hellerman–Rosenstein \(1983\)](#) wind stress



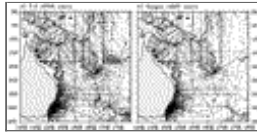
[Click on thumbnail for full-sized image.](#)

FIG. 2. Bottom topography of the region studied. Light and dark shading is used to indicate areas where water depth is shallower than 100 and 1000 m, respectively. Solid lines indicate 2000 -m isobath



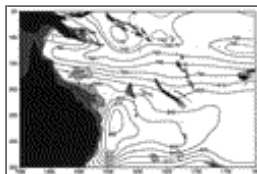
[Click on thumbnail for full-sized image.](#)

FIG. 3. Dynamics heights (dyn cm) relative to 1200 db calculated from the *World Ocean Atlas 1998*. The region of interest for this study is shaded



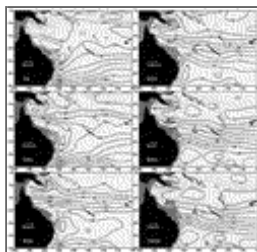
[Click on thumbnail for full-sized image.](#)

FIG. 4. Geographical distribution of stations (asterisk) of (a) temperature–salinity and (b) oxygen used in this study. Solid lines indicate 100-m isobath



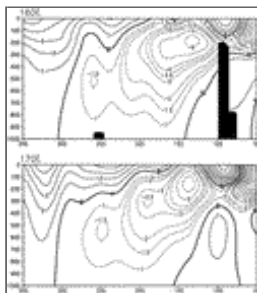
[Click on thumbnail for full-sized image.](#)

FIG. 5. Depth-integrated (0–1000 m) dynamic height (m^2) relative to 1200 db. The light and dark shading denotes areas where water depth is shallower than 100 and 1000 m, respectively



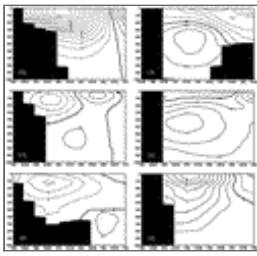
[Click on thumbnail for full-sized image.](#)

FIG. 6. Dynamic heights (dyn cm) and geostrophic velocities (cm s^{-1}) relative to 1200 db at 0, 100, 300, 500, 800, and 1000 m



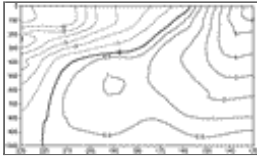
[Click on thumbnail for full-sized image.](#)

FIG. 7. Geostrophic velocities (cm s^{-1}) at 160° and 170°E . Positive values are eastward. Contour interval is 1 cm s^{-1} , with additional counters of -1.5 and -3.5 cm s^{-1}



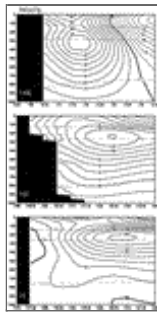
Click on thumbnail for full-sized image.

FIG. 8. Geostrophic velocity (cm s^{-1}) along the western boundary at 23°, 21°, 19°, 17°, 15°, and 13°S. Positive values are northward



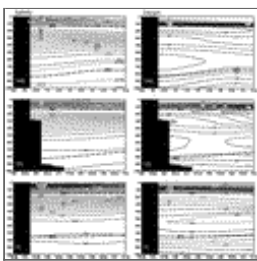
Click on thumbnail for full-sized image.

FIG. 9. Alongshore velocity (cm s^{-1}) averaged within 2° from the coast. Positive values are northwestward, and the contour of zero velocity indicates the bifurcation of the SEC



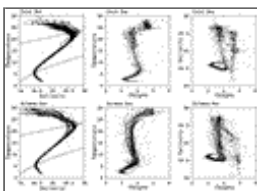
Click on thumbnail for full-sized image.

FIG. 10. Geostrophic velocity (cm s^{-1}) south of New Guinea at 149°E, around the Louisiade at 10°S, and in the Solomon Sea at 7°S. The geographic locations of these sections are indicated in [Fig. 2](#). Positive values are eastward in meridional section and northward in zonal sections. Light dashed lines indicate 24.5, 26.0, and 27.2 σ_θ surfaces.



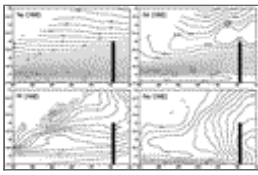
Click on thumbnail for full-sized image.

FIG. 11. Same as [Fig. 10](#) except for salinity (psu) and oxygen concentration (ml l^{-1}) against depth (m)



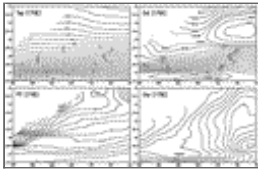
Click on thumbnail for full-sized image.

FIG. 12. Relations of temperature vs salinity, temperature vs oxygen concentration, and salinity vs oxygen concentration in the Coral Sea and Solomon Sea. The solid lines on the left panels indicate 24.5 and 27.2 σ_θ surfaces



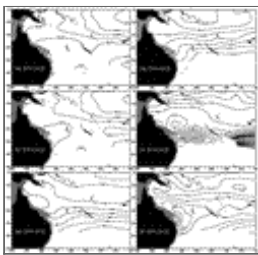
[Click on thumbnail for full-sized image.](#)

FIG. 13. Vertical sections of potential temperature (°C), salinity (psu), potential vorticity ($10^{-10} \text{ m}^{-1} \text{ s}^{-1}$), and dissolved oxygen concentration (ml l^{-1}) along 160°E . Here potential vorticity has been multiplied by a factor of -1 before plotting



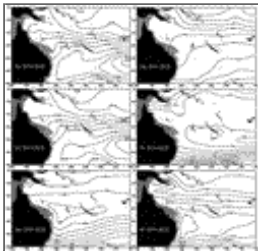
[Click on thumbnail for full-sized image.](#)

FIG. 14. Same as [Fig. 13](#) except along 170°E



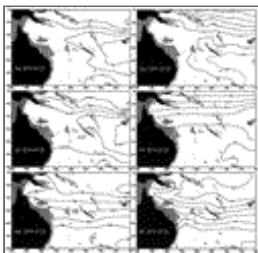
[Click on thumbnail for full-sized image.](#)

FIG. 15. Distributions of potential temperature (°C), salinity (psu), isopycnal depth (m), dissolved oxygen concentration (ml l^{-1}), potential vorticity ($10^{-10} \text{ m}^{-1} \text{ s}^{-1}$), and acceleration potential ($\text{m}^2 \text{ s}^{-2}$) in the western South Pacific along 24.5 , 26.0 , and $27.2 \sigma_\theta$ surfaces. Potential vorticity has been multiplied by a factor of -1 before plotting



[Click on thumbnail for full-sized image.](#)

FIG. 15. (*Continued*)



[Click on thumbnail for full-sized image.](#)

FIG. 15. (*Continued*)

top ▲



© 2008 American Meteorological Society [Privacy Policy and Disclaimer](#)

Headquarters: 45 Beacon Street Boston, MA 02108-3693

DC Office: 1120 G Street, NW, Suite 800 Washington DC, 20005-3826

amsinfo@ametsoc.org Phone: 617-227-2425 Fax: 617-742-8718

[Allen Press, Inc.](#) assists in the online publication of *AMS* journals.